On cascades of resonators for high-bandwidth integrated optical interconnection networks

Benjamin A. Small, Benjamin G. Lee, and Keren Bergman

Columbia University Department of Electrical Engineering, New York 10027

Abstract: The power penalty characteristics of high-speed optical signals transmitted through a variety of filters based on multiple microring resonator devices are analyzed by numerical simulation. The technique used here has been verified with single-ring experimental measurements. Butterworth and Chebyshev filters are investigated, as are serial cascades of resonant devices. Although the power penalty is generally not prohibitive, it is a parameter which cannot be ignored for the design of complex high-bandwidth photonic interconnect systems that utilize microring resonators as filters and switches.

©2006 Optical Society of America

OCIS Codes: (230.5750) Resonators; (230.3120) Integrated optics devices; (060.4510) Optical communications.

References and links

1. K. J. Vahala, "Optical microcavities," Nature **424**, 839–846 (2003).
2. B. E. Little, S. T. Chu, H. A. Haus, J. Foresi, and J. P. Laine, "Microring resonator channel dropping filters," J. Lightwave Technol. **15**, 998–1005 (1997).
3. C. Manolatou, M. J. Khan, S. Fan, P. R. Villeneuve, H. A. Haus, and J. D. Joannopoulos, "Coupling of modes analysis of resonant channel add-drop filters," IEEE J. Quantum Electron. **35**, 1322–1331 (1999).
4. M. Lipson, "Guiding, modulating, and emitting light on silicon–challenges and opportunities," J. Lightwave Technol. **23**, 4222–4238 (2005).
5. B. A. Small, B. G. Lee, K. Bergman, Q. Xu, J. Shakya, and M. Lipson, "High data rate signal integrity in micron-scale silicon ring resonators," in *Proc. CLEO*, paper CTuCC4 (2006).
6. B. G. Lee, B. A. Small, K. Bergman, Q. Xu, and M. Lipson, "Transmission of high-data-rate optical signals through a micrometer-scale silicon ring resonator," Opt. Lett. **31** (2006).
7. B. Zhang, D. Leuenberger, M.-C. M. Lee, S. Hu1, M. Haghi1, A. E. Willner, and M. C. Wu, "Error-free data transmission through a tunable-bandwidth filter based on MEMS-actuated microdisk resonator," in *Proc. CLEO*, paper CFC3 (2006).
8. M. Pfennigbauer, M. M. Strasser, M. Pauer, P. J. Winzer, "Dependence of optically preamplified receiver sensitivity on optical and electrical filter bandwidths-measurement and simulation," IEEE Photon. Technol. Lett. **14**, 831–833 (2002).
9. G. P. Agrawal, *Fiber-Optic Communication Systems*, 3rd ed. (Wiley, New York, 2002).
10. C. J. Kaalund and G.-D. Peng, "Pole-zero diagram approach to the design of ring resonator-based filters for photonic applications," J. Lightwave Technol. **22**, 1548–1559 (2004).
11. Q. Xu, B. Schmidt, S. Pradhan, and M. Lipson, "Micrometre-scale silicon electro-optic modulator," Nature **435**, 325-327 (2005).
12. V. R. Almeida, C. A. Barrios, R. R. Panepucci, and M. Lipson, "All-optical control of light on a silicon chip," Nature **431**, 1081–1084 (2004).
13. R. B. Blackman and J. W. Tukey, *The Measurement of Power Spectra, from the Point of View of Communications Engineering* (Dover, New York, 1959).
14. E. W. Kamen and B. S. Heck, Fundamentals of Systems and Signals, 2nd ed. (Prentice-Hall, Englewood Cliffs, 2000).
15. A. Yariv, Y. Xu, R. K. Lee, and A. Scherer, "Coupled resonator optical waveguides: a proposal and analysis," Opt. Lett. **24**, 711–713 (1999).
16. J. V. Hryniewicz, P. P. Absil, B. E. Little, R. A. Wilson, and P.-T. Ho, "Higher order filter response in coupled microring resonators," IEEE Photon. Technol. Lett. **12**, 320–322 (2000).
17. Y. Yanagase, S. Suzuki, Y. Kokubun, and S. T. Chu, "Box-like filter response and expansion of FSR by a vertically triple coupled microring resonator filter," J. Lightwave Technol. **20**, 1525–1529 (2002).
18. A. Agarwal, P. Toliver, R. Menendez, S. Etemad, J. Jackel, J. Young, T. Banwell, B. E. Little, S. T. Chu, W. Chen, W. Chen, J. Hryniewicz, F. Johnson, D. Gill, O. King, R. Davidson, K. Donovan, and P. J. Delfyett, "Fully programmable ring-resonator-based integrated photonic circuit for phase coherent applications," J. Lightwave Technol. **24**, 77–87 (2006).

#71820 - $15.00 USD Received 12 June 2006; revised 21 August 2006; accepted 20 September 2006

19. P. Koonath, T. Indukuri, and B. Jalali, "Monolithic 3-D silicon photonics," J. Lightwave Technol. **24**, 1796–1804 (2006).
20. F. Xia, L. Sekaric, and Y. A. Vlasov, "Mode conversion losses in silicon-on-insulator photonic wire based racetrack resonators," Opt. Express **14**, 3872–3886 (2006).

1. Introduction

Photonic microcavity devices which exhibit sharp spectral features due to resonant recirculation have received significant attention recently [1]. These devices have the potential to be used as ultra-narrow filters and as photonic switching elements in monolithic high-bandwidth photonic integrated circuits (PICs) [1–4]. Although the sharp spectral features of these devices can easily be leveraged for ultra-dense wavelength division multiplexing (DWDM) and for high-speed wavelength-selective switching, it has been shown that the sidebands of optical signals with high data rates can be affected, resulting in signal distortion [5–8]. This can be problematic for systems, such as high-bandwidth integrated optical interconnects and high-density optical telecommunications systems, which would contain many of these devices (e.g. reconfigurable add/drop multiplexers and switching elements) in cascade.

Signal degradation can be easily quantified by the power penalty, which is a metric commonly used in optical telecommunications systems and expresses the amount of additional receiver power required to overcome the signal errors introduced by a particular device or subsystem [9]. This investigation considers different laterally side-coupled configurations of microring resonators which can realize well-known filter structures [10] and evaluates their power penalty characteristics, using a verified numerical simulation technique, which has shown agreement of better than 7 % with experimental measurements for single-resonator systems [5, 6]. Series cascades of microring resonator filters within multiple-stage systems are explored as well. Because it has been proposed that microring resonator devices can also be leveraged as electro-optic [11] and all-optical [12] switching devices, these analyses consider both the power penalty introduced by resonators and an approximation of the switching ratio that could be achieved. This study concludes that the design of microring resonator-based photonic circuits requires a nuanced and thorough understanding of the effects these devices have on high-speed optical signals.

2. Simulation model

The authors have introduced a technique for simulating the signal degradation and power penalty induced by spectrally narrow microring resonator devices and have verified its accuracy experimentally [5, 6]. Those results confirmed that the amplitude distortion of signal sidebands dominates phase distortion and dispersion as the primary source of power penalty. This model, therefore, captures the nonuniform attenuation of the modulation sidebands of a high-speed optical signal based on resonant devices' fine spectral characteristics [13, 14]. When an optical signal is routed through the drop port of a microring resonator, the higher-order modulation sidebands are attenuated more than the lower-order ones, resulting in transition smoothing, extinction ratio degradation, and other signal distortions [5,6]. The best possible extinction ratio ε can be related to the calculated power penalty δ by [9]:

$$\delta = \frac{\varepsilon + 1}{\varepsilon - 1}. \tag{1}$$

This is the power penalty figure used in the following analysis and represents the best possible power penalty, assuming an ideal amplifier. For practical systems, additional power penalty should be included, depending upon on the noise characteristics of a particular amplifier, filter bandwidth, and overall signal attenuation.

When the carrier wavelength is detuned from the center of the resonance spectrum, additional signal attenuation is observed, and asymmetry can lead to further signal degradation. The present investigation contains relationships which have been distilled from data generated by previously verified numerical simulations [5, 6].

#71820 - $15.00 USD Received 12 June 2006; revised 21 August 2006; accepted 20 September 2006
(C) 2006 OSA

For this analysis, frequency is given as a unitless parameter: the ratio of the full-width at half-maximum (FWHM) Γ of microring resonator-based filters to the data rate F of the optical signal is used. Thus, a Γ/F ratio of 1.2 indicates, for example, that a 10 Gbps optical signal is transmitted through a device with a FWHM of 12 GHz (96 pm), or Q of approximately 16,000 for a carrier wavelength in the middle of the C-band (1550 nm); or a 40 Gbps optical signal and a FWHM of 48 GHz (386 pm), or Q of 4000. For all simulations, the optical signal is assumed to be amplitude-modulated with a continuous stream of random non-return to zero (NRZ) data.

3. Single resonator

The simplest possible filter transmission characteristic is a Lorentzian (Cauchy) lineshape:

$$T(f) = \frac{1}{(2f/\Gamma)^2 + 1}. \tag{2}$$

This kind of filter requires only a single microring resonator device. In this case, the only filter parameter is the spectral ratio Γ/F; the detuning of the carrier wavelength from the center of the resonance spectrum is also normalized to the optical signal bandwidth, $\Delta f/F$.

Both the attenuation in total transmitted power α and the power penalty δ are characterized as they vary with the detuning of the optical signal carrier wavelength from the center of the resonance spectrum (Fig. 1). As expected, overall signal attenuation increases with decreasing FWHM (increasing Q). Furthermore, signal degradation, as quantified by the power penalty, increases with decreasing FWHM as well, since greater sideband attenuation is experienced. Symmetrically, with greater detuning of the carrier wavelength, both attenuation and power penalty generally increase as well.

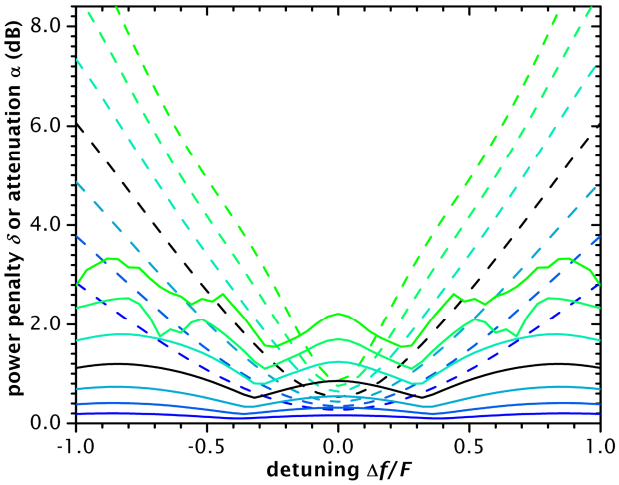

Fig. 1. Power penalty (solid curve) and attenuation (dashed curve) for Lorentzian filters with Γ/F between ½ (green) and 2 (blue), logarithmically; black curves for $\Gamma = F$.

The power penalty curves have minima at nonzero detuning values, which at first may be unexpected. Consider, however, that for an entirely real function $g(x)$, $\mathrm{Im}\{g(x)\} = 0$, the Fourier transform $G(\omega) = \mathcal{F}\{g(x)\}$ is conjugate-symmetric: $G(-\omega) = G(\omega)^*$. Therefore, only half of the Fourier spectrum is required to decode the correct time-domain signal. It is also interesting to note that each lobe of the Fourier spectrum of a continuous stream of NRZ data is roughly bounded by a triangle [13,14]. In order to determine the detuning Δf which results in the most total power from one half of the fundamental spectral lobe, approximated as a

#71820 - $15.00 USD Received 12 June 2006; revised 21 August 2006; accepted 20 September 2006
(C) 2006 OSA

triangle, when multiplied by the Lorentzian filter shape (Fig. 2 inset), consider the convolution integral:

$$\int_{\Delta f-1}^{\Delta f} \frac{(f-\Delta f+1)}{(2f/\Gamma)^2+1}\,df = \frac{1-\Delta f}{2}\arctan\left[\frac{2\Gamma}{\Gamma^2+4\Delta f^2-4\Delta f}\right]\Gamma + \frac{1}{8}\log\left[\frac{\Gamma^2+4\Delta f^2}{\Gamma^2+4(1-\Delta f)^2}\right]\Gamma^2. \quad (3)$$

The maxima indicated by this convolution function and the minima observed as a result of the numerical simulation of the power penalty for a Lorentzian filter agree fairly well (Fig. 2); the error at $\Gamma = F$ is just 8 %. Even this simplistic analysis illustrates that minima in the power penalty curves are expected to be at nonzero values of detuning for certain filter shapes.

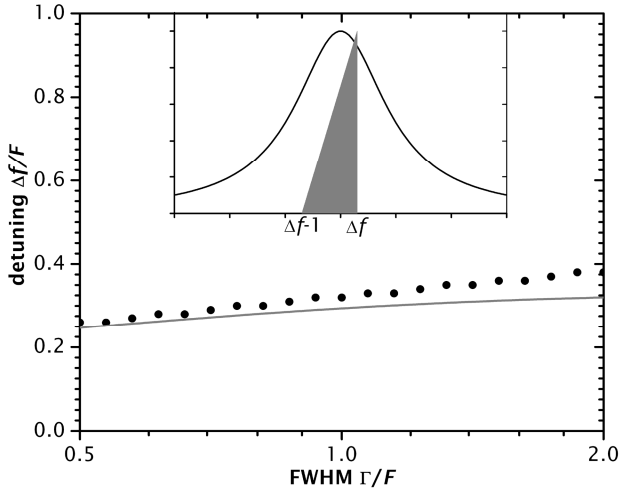

Fig. 2. Comparison between detuning values at observed power penalty minima (points) and predicted maximum signal integrity from Eq. (3) (curve); the inset is a sketch of the simplistic estimation upon which Eq. (3) is based.

When using a microring resonator device as a modulator or as a switch, the resonance spectrum is shifted so that a particular wavelength changes from being on-resonance to being off-resonance, or vice versa [11, 12]. This shift in the resonance spectrum is generally on the order of the FWHM itself. The best-case switching ratio (or extinction ratio for a modulator device) can therefore be estimated by the ratio of the induced attenuation:

$$R = \frac{\alpha(\Delta f = F)}{\alpha(\Delta f = 0)}. \quad (4)$$

The shape and steepness of the overall attenuation curve manifested by a particular filter can be of great interest for system applications.

4. Filter design

Other kinds of filters can be implemented with microring resonators as well, by utilizing appropriate waveguide geometries to design the critical coupling relationship for each resonator [10]. The transmission characteristics of any of these arrangements can be expressed as

$$T(f) = \frac{1}{\left[P(2f/\Gamma)\right]^2+1}, \quad (5)$$

wherein $P(\bullet)$ is the appropriate polynomial (generally special cases of the Jacobi polynomials). For the Lorentzian described above, $P(z) = z$. The most commonly found linear filter types are the Butterworth filter (i.e. maximally flat filter) and the type-I Chebyshev filter (hereafter simply "Chebyshev" since type-II filters are not discussed). For an *n*th-order

#71820 - $15.00 USD Received 12 June 2006; revised 21 August 2006; accepted 20 September 2006
(C) 2006 OSA

Chebyshev filter, P(•) is an *n*th-order Chebyshev polynomial of the first kind, for which *n* resonators are required. For an *n*th-order Butterworth filter, where $P(z) = z^n$, *n* resonators are also required. Thus, a Lorentzian, as in Eq. (2), is both a first-order Chebyshev and a first-order Butterworth filter (Fig. 3).

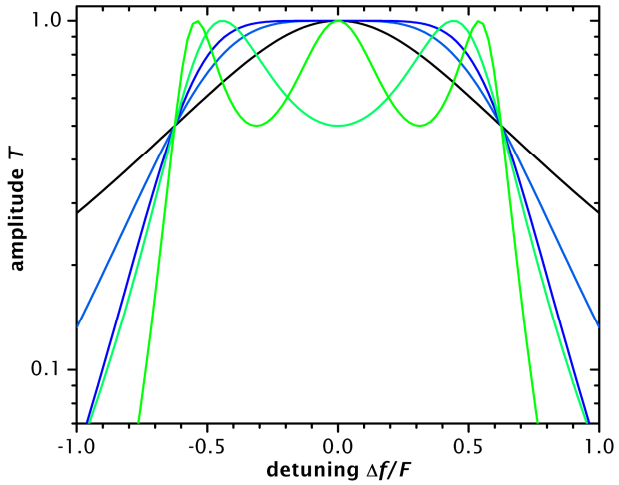

Fig. 3. Comparison of filter shapes with $\Gamma/F = 1.25$, Lorentzian or first-order (black), second- and third-order Butterworth (blue), and second- and third-order Chebyshev (green).

It is common practice to utilize a transverse cascade of side-coupled microring resonators to implement filters with relatively flat transmission characteristics and good channel isolation (i.e. low shape factor) [2, 10, 15–20]. These filters are often designed to be even-order Butterworth filters, although fabrication imperfections can alter the transmission characteristics slightly. Both overall signal attenuation and power penalty are characterized for Butterworth filters (Fig. 4) and Chebyshev filters (Fig. 5). As expected, Butterworth filters have flatter power penalty curves (lower shape factor), resulting from the relatively more uniform transmission spectrum. Although the Chebyshev filters induce very uneven power penalty which depends strongly on detuning, they offer the potential for better switching ratios, as enunciated in Eq. (4), and may be better suited for modulators and switching applications. For example, a third-order Butterworth filter with $\Gamma/F = 1.25$ has $R = 3.6$ (5.6 dB), whereas for a third-order Chebyshev filter with the same FWHM, $R = 4.2$ (6.2 dB), while also having a steeper attenuation curve.

#71820 - $15.00 USD Received 12 June 2006; revised 21 August 2006; accepted 20 September 2006
(C) 2006 OSA

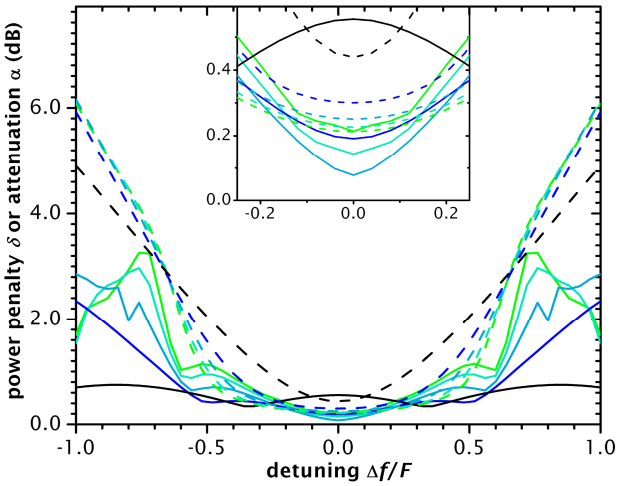

Fig. 4. Power penalty (solid lines) and attenuation (dashed lines) for Butterworth filters with I'/F = 1.25, from second-order (blue) to fifth-order (green); black curves for Lorentzian; inset of region near origin.

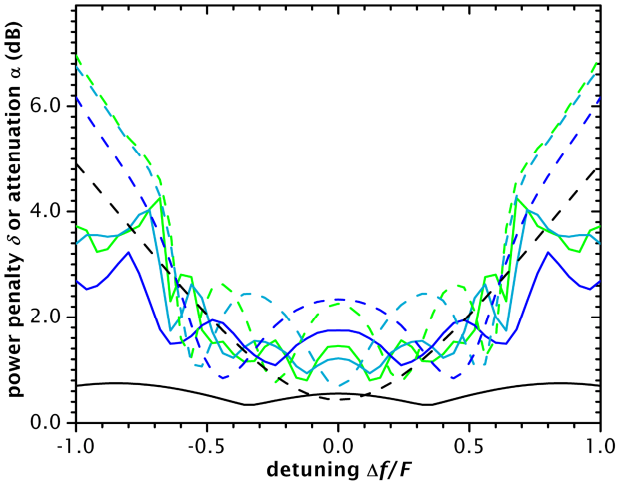

Fig. 5. Power penalty (solid lines) and attenuation (dashed lines) for Chebyshev filters with I'/F = 1.25, from second-order (blue) to fourth-order (green); black curves for Lorentzian.

It is interesting to note that the Butterworth filter which yields the lowest power penalty value is not necessarily the highest-order one. This is because of the complex behavior resulting from the extreme sideband attenuation induced by higher-order filters, even though the middle of the filters offer maximally flat transmission characteristics. The optimal order for a Butterworth filter depends on the precise FWHM value (Fig. 6); having more resonators is not necessarily better for power penalty. This relationship is important when considering the tradeoffs between device footprint and channel isolation for system design.

#71820 - $15.00 USD Received 12 June 2006; revised 21 August 2006; accepted 20 September 2006
(C) 2006 OSA

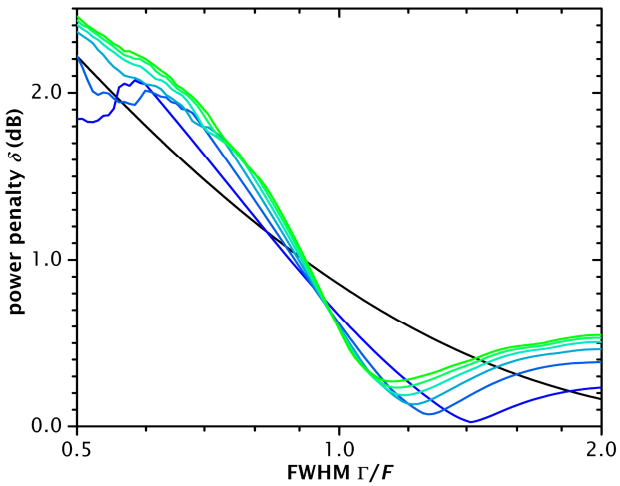

Fig. 6. Power penalty at zero detuning ($\Delta f = 0$) with different values of FWHM for Butterworth filters, from second-order (blue) to fifth-order (green); black curve for Lorentzian.

5. Resonator cascades

Another important situation to consider is a complex optical communications system which requires signals to traverse multiple microring resonator devices for filtering and switching. Although the integrity of an optical signal is unaffected by exiting the through port of a resonant device, propagation through multiple resonator drop ports could result in significant signal degradation. In this case, the net transmission spectrum becomes narrower with each successive resonator and does not maintain a Lorentzian shape (Fig. 7). Serial cascades of resonators, as in a system, should not be confused with side-coupled resonators which can be used to tailor a single complex filter; in this case the devices are assumed to be independent and isolated from each other.

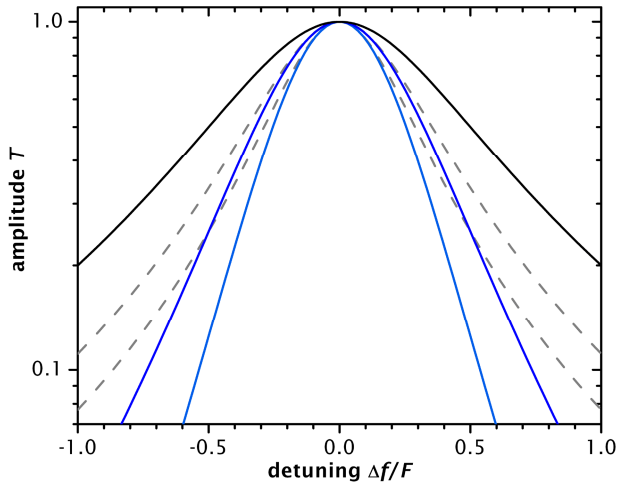

Fig. 7. Comparison of filter shapes with $\Gamma/F = 1.25$, single first-order filter (black), cascades of two and three successive devices (blue); Lorentzian lineshapes with FWHM scaled by $\sqrt{2}/2$ and $\sqrt{3}/3$ are given for reference (gray dashed curves).

Accordingly, both overall signal attenuation and power penalty are characterized for serial cascades of simple Lorentzian filters (Fig. 8). Unfortunately, these cascades demonstrate

#71820 - $15.00 USD Received 12 June 2006; revised 21 August 2006; accepted 20 September 2006
(C) 2006 OSA

progressively less intolerance to detuning; both the power penalty and the overall attenuation vary significantly from their respective zero-detuning values.

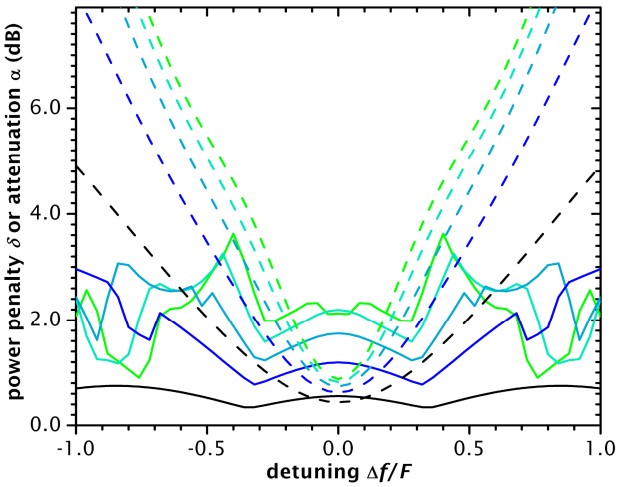

Fig. 8. Power penalty (solid lines) and attenuation (dashed lines) for serial cascades of first-order filters with $\Gamma/F = 1.25$, from two (blue) to five (green); black curves for a single device.

6. Conclusions

The power penalty which is induced on an optical signal due to sideband attenuation encountered in microring resonator devices with narrow spectral features is a complex parameter. Typically ranging from 0.2 dB to 2.0 dB, depending on the particular filter characteristics, this power penalty is a noticeable but not limiting factor for system design. It can be controlled to some extent by tailoring the filter characteristics using multiple resonant devices. This investigation concludes through numerical simulations of sideband attenuation effects that filters which contain more microring resonators (high-order) are not necessarily better for signal quality than ones which contain fewer, and that Butterworth filter types may provide the best power penalty characteristics while Chebyshev ones may be more suited for switching applications. The additional signal degradation resulting from serial cascades of resonant devices is also introduced.

When leveraging this technology for switching and modulation, both the overall attenuation experienced by a high-speed optical signal and the power penalty resulting from sideband attenuation are important. Thoroughly understanding all of the design implications of complex filters and serial cascades of multiple devices is critical for the design of high-bandwidth PICs which leverage this technology.

Acknowledgments

The authors would like to acknowledge the support of the National Science Foundation under grants CCF-0523771 and ECS-0532762. They would also like to thank Qianfan Xu and Michal Lipson of Cornell University.

#71820 - $15.00 USD Received 12 June 2006; revised 21 August 2006; accepted 20 September 2006
(C) 2006 OSA